Potential Vorticity Balances and Horizontal Divergence along Particle Trajectories in Gulf Stream Meanders East of Cape Hatteras

AMY S. BOWER*

Graduate School of Oceanography, University of Rhode Island, Narragansett, Rhode Island

(Manuscript received 18 July 1988, in final form 17 April 1989)

ABSTRACT

Trajectories of 37 isopycnal RAFOS floats launched in the Gulf Stream off Cape Hatteras have been analyzed to examine the dynamics of meanders from a Lagrangian viewpoint. Using the float data in conjunction with information on the structure of horizontal velocity shear from the PEGASUS study (Halkin and Rossby), variations in planetary, curvature, and shear vorticity have been estimated along the float trajectories. Changes in fluid layer thickness were then inferred assuming potential vorticity is conserved following the floats.

This analysis shows that curvature vorticity changes are typically 10%–20% of f (planetary vorticity) as fluid parcels travel between meander troughs and crests. Lateral shear changes on the order of 20%–30% of f are common as parcels move laterally relative to the jet axis between meander extrema. Although changes in these two terms are usually of opposite sign and tend to compensate, significant layer thickness changes do occur, with some parcels exhibiting 30% changes in thickness over several days.

Sixty-one estimates of horizontal divergence were made from the average time rate of change of layer thickness between meander extrema. The magnitude of horizontal divergence [$O(.01f)$] was found to be a strong function of temperature, clearly decreasing with decreasing temperature through the main thermocline.

Even more striking was the dependence of the sign of horizontal divergence on cross-stream position. On the anticyclonic side of the stream, divergence (convergence) was indicated downstream of a trough (crest). On the cyclonic side, convergence (divergence) was present downstream of a trough (crest). These results are discussed in relation to the free inertial jet model of the Gulf Stream developed by Robinson and Niiler. Implications for quasi-geostrophic theory are examined and it is found that this approximation may not be appropriate for use in the Gulf Stream.

1. Introduction

The Gulf Stream east of Cape Hatteras is characterized by large-amplitude meanders that grow and progress downstream. In these strongly curved sections of the current, centripetal acceleration becomes a significant term in the cross-stream momentum balance. The ratio of centripetal to Coriolis acceleration, or the curvature Rossby number, can be on the order of 0.2 in the surface waters, indicating that the flow deviates substantially from geostrophic balance.

Meteorologists have been aware of the importance of centripetal acceleration in the balanced curved flow of the upper-level atmospheric jet stream for some time (e.g., Bjerknes and Holmboe 1944; Palmen and Newton 1969). They have found that changing curvature along the path of the jet stream causes significant convergence and divergence in the flow field. In particular, upper-level divergence which occurs downstream of a trough or cyclonic loop in the jet stream's path, leads to uplifting throughout the underlying air column and subsequent lower-level convergence near the earth's surface (for example, see Holton 1979). Thus the structure of vertical motion and divergence is tightly linked to the meandering pattern of the jet.

The Gulf Stream is somewhat analogous to the jet stream; both are meandering baroclinic jets with, as Newton (1978) has pointed out, comparable lateral and vertical velocity shears and cross-frontal slope of isotherms. It seems plausible therefore, that the convergence and divergence pattern which is ubiquitous in the waves of the atmospheric jet stream may be present to some degree in Gulf Stream meanders as well.

In this study, divergence and convergence in the Gulf Stream will be studied from an observational viewpoint. Using a recently developed subsurface isopycnal drifter called the RAFOS float, the variations in the terms of potential vorticity along a fluid parcel trajectory can be estimated. One of these terms in particular, the vortex stretching of the parcel, which is related to horizontal divergence, will be studied to investigate how the structure of vertical motion and divergence is linked to meandering of the Gulf Stream path. The RAFOS float is uniquely suited for such a study due to its constant density capability, which allows it to follow the

* Present affiliation: Woods Hole Oceanographic Institution.

Corresponding author address: Dr. Amy S. Bower, Woods Hole Oceanographic Institution, Woods Hole, MA 02543.

vertical motion of fluid parcels along sloping density surfaces in the Gulf Stream. The floats are rendered isopycnal by the attachment of a spring-backed piston which gives the float package nearly the same compressibility as seawater (see Rossby et al. 1985, for more details).

Thirty-seven of these drifters were launched sequentially in the main thermocline of the Gulf Stream off Cape Hatteras between January 1984 and October 1985. The floats were tracked underwater acoustically relative to three moored sound sources. Pressure, temperature, and an acoustic position fix were recorded by each float every 8 hours for 30 or 45 days, depending on the length of the mission, after which the float popped to the surface and transmitted the collected data to the ARGOS satellite tracking system. A more complete description of the RAFOS float and its navigation system is given by Rossby et al. (1986).

A kinematic analysis of this dataset in a companion paper by Bower and Rossby (1989, hereafter BR) revealed a striking pattern of motion which is directly correlated to changes in curvature along the stream path. Fluid parcels systematically upwell and move onshore downstream of meander troughs and downwell and move offshore downstream of crests.

In this study, the focus will be on the dynamics of the flow following these floats. Using the float data in conjunction with detailed information on the cross-stream structure of the Gulf Stream from the PEGASUS velocity study at 73°W by Halkin and Rossby (1985, hereafter HR), the important components of potential vorticity can be estimated along the float trajectories. Two of these components, planetary and curvature vorticity, were estimated from the float data. (Trajectory curvature was converted to streamline curvature using the mean phase propagation rate for meanders in this region.) Lateral shear vorticity was estimated with the aid of the PEGASUS study and vortex stretching was estimated as a residual by taking advantage of the potential vorticity conservation constraint following a parcel. We then relate the structure of vortex stretching (and associated horizontal divergence) to the meandering path of the Gulf Stream.

In the next section, a review of the methodology will be given, including a thorough consideration of the estimated uncertainties. The results are presented in section 3, first in the form of time series of the potential vorticity components for two floats, and then in the form of divergence estimates in meanders of the stream using all the floats. These observations are discussed in section 4 in relation to the free inertial jet model of Robinson and Niiler (1967).

2. Methodology

a. *Potential vorticity in the Gulf Stream*

In order to examine the various components of potential vorticity in the Gulf Stream using the RAFOS observations, it is necessary to get the potential vorticity equation in a form which is suitable for use with the floats. We begin with Ertel's (1942) theorem, which states that the potential vorticity of a fluid parcel will be conserved along its trajectory when dissipative effects are negligible (see appendix A for estimate of eddy diffusive terms);

$$\frac{d}{dt}\left(\vec{\zeta}_a \cdot \frac{\nabla\rho}{\rho}\right) = 0 \tag{1}$$

where

$\vec{\zeta}_a$ absolute vorticity,
$\nabla\rho$ density gradient,
$(d/dt)(\ )$ $(\partial/\partial t)(\ ) + \mathbf{V}\cdot\nabla(\ )$, the substantial derivative,
$\mathbf{V}$ velocity vector.

When applying this equation to the Gulf Stream, it is convenient to use a natural coordinate system where x is the cross-stream coordinate (positive offshore), y is the along-stream coordinate (positive downstream), and z is the vertical coordinate (positive upward). If the expression in parentheses is transformed to this natural coordinate system and scaled using the values in Tables 1 and 2, the following terms remain,

$$-\frac{1}{\rho}\frac{\partial\rho}{\partial x}\frac{\partial v}{\partial z} + \frac{1}{\rho}\frac{\partial\rho}{\partial z}\left(f + \frac{\partial v}{\partial x} + \kappa_s v\right) = \text{const.} \tag{2}$$

Here $\kappa_s v$ is the curvature vorticity (part of relative vorticity in natural coordinates where κ_s is streamline curvature). The gradients of density and downstream velocity in Table 1 were estimated using the mean tem-

TABLE 1. Magnitude of terms used in scaling analysis of potential vorticity equation.

$$\frac{1}{\rho}\frac{\partial\rho}{\partial x} \approx \frac{1}{1\ \text{g cm}^{-3}}\frac{0.00075\ \text{g cm}^{-3}}{40\ \text{km}} = 0.02\times10^{-8}\ \text{cm}^{-1}$$

$$\frac{1}{\rho}\frac{\partial\rho}{\partial y} \approx \frac{1}{1\ \text{g cm}^{-3}}\frac{.0003\ \text{g cm}^{-3}}{200\ \text{km}} = 1\times10^{-11}\ \text{cm}^{-1}$$

$$\frac{1}{\rho}\frac{\partial\rho}{\partial z} \approx \frac{1}{1\ \text{g cm}^{-3}}\frac{0.0013\ \text{g cm}^{-3}}{500\ \text{m}} = 2.5\times10^{-8}\ \text{cm}^{-1}$$

$$h_x, h_y, f \approx 1\times10^{-4}\ \text{s}^{-1}$$

$$\frac{\partial w}{\partial y} \approx \frac{0.1\ \text{cm s}^{-1}}{200\ \text{km}} = 5\times10^{-9}\ \text{s}^{-1}$$

$$\frac{\partial v}{\partial z} \approx \frac{50\ \text{cm s}^{-1}}{450\ \text{m}} = 1\times10^{-3}\ \text{s}^{-1}$$

$$\frac{\partial w}{\partial x} \approx \frac{0.1\ \text{cm s}^{-1}}{40\ \text{km}} = 2.5\times10^{-8}\ \text{s}^{-1}$$

$$\frac{\partial v}{\partial x} \approx \frac{100\ \text{cm s}^{-1}}{40\ \text{km}} = 2.5\times10^{-5}\ \text{s}^{-1}$$

$$\kappa_s v \approx \frac{1}{100\ \text{km}}\,100\ \text{cm s}^{-1} = 1\times10^{-5}\ \text{s}^{-1}$$

TABLE 2. Relative magnitudes of terms in potential vorticity equation.

Term	Magnitude relative to $\frac{1}{\rho}\frac{\partial \rho}{\partial z} f$
$\frac{1}{\rho}\frac{\partial \rho}{\partial x} h_x$	8×10^{-3}
$\frac{1}{\rho}\frac{\partial \rho}{\partial x}\frac{\partial w}{\partial y}$	5×10^{-7}
$\frac{1}{\rho}\frac{\partial \rho}{\partial x}\frac{\partial v}{\partial z}$	1×10^{-1}
$\frac{1}{\rho}\frac{\partial \rho}{\partial y} h_y$	5×10^{-4}
$\frac{1}{\rho}\frac{\partial \rho}{\partial y}\frac{\partial w}{\partial x}$	1×10^{-7}
$\frac{1}{\rho}\frac{\partial \rho}{\partial z} f$	1×10^{0}
$\frac{1}{\rho}\frac{\partial \rho}{\partial z}\frac{\partial v}{\partial x}$	2.5×10^{-1}
$\frac{1}{\rho}\frac{\partial \rho}{\partial z} \kappa_s v$	1×10^{-1}

perature and velocity sections from the PEGASUS study (HR; see also Fig. 1), while the gradients of vertical velocity were estimated based on the observations described by BR. In this study, terms which are less than 1% of the leading term,

$$\frac{1}{\rho}\frac{\partial \rho}{\partial z} f,$$

are considered to be of second order and will not be retained.

To put the potential vorticity equation in an appropriate form for use with the constant density RAFOS floats, the x and z axes are rotated slightly such that the cross-stream coordinate (now called n) is directed along the density surfaces. Although the magnitudes of f, the vertical component of planetary vorticity, and $\rho^{-1}\partial\rho/\partial z$, the vertical stratification, in the rotated frame are not exactly equivalent to the values of these terms in the non-rotated frame, differences are less than 1% for a cross-stream isopycnal slope of 0.01, typical for the Gulf Stream main thermocline. In this transformation the first term in Eq. (2) is absorbed into the second term and the expression for potential vorticity becomes

$$\frac{f + \dfrac{\partial v}{\partial n} + \kappa_s v}{H} = \text{const} \qquad (3)$$

where $\partial v/\partial n$ now represents the lateral shear along a *density* surface. In addition, H, the vertical distance between two specified density surfaces, has replaced $\rho^{-1}\partial\rho/\partial z$.

b. *Estimation of potential vorticity terms following RAFOS floats*

In this study the lateral shear following the RAFOS floats was modeled using information from the PEGASUS study, while H was estimated as a residual. Conceivably, one could have modeled the density stratification instead and estimated changes in shear as a residual. In this case, however, uncertainty in estimating H from a model would lead to an uncertainty in the residual estimate of $\partial v/\partial n$ on the order of f. Since $\partial v/\partial n$ is a small fraction of f in the main thermocline of the Gulf Stream, the changes in $\partial v/\partial n$ we are trying to detect would be less than the estimated uncertainty. For this reason, we have chosen to model the velocity structure along density surfaces using the mean velocity section in natural coordinates established by HR and estimate H as a residual. Each term in potential vorticity was estimated as described below.

1) PLANETARY VORTICITY TERM

The planetary vorticity, f, is easily estimated along the float trajectories from the acoustic position fixes obtained every 8 hours. Due to variations in sound propagation and timing uncertainties, the measurement uncertainty in position is about ±5 km. The associated uncertainty in f is given by $\sigma_f = \beta\sigma_y$, where β is the change in f with latitude, and σ_y is the position uncertainty—with $\beta = 2 \times 10^{-13}$ cm^{-1} s^{-1} and $\sigma_y = \pm 5$ km, $\sigma_f = \pm 0.01 \times 10^{-5}$ s^{-1}.

2) CURVATURE VORTICITY TERM

In order to estimate curvature vorticity ($\kappa_s v$) following the RAFOS floats, it was first necessary to convert the curvature of the float's trajectory (κ_t) to streamline curvature (κ_s). This was accomplished using Blaton's formula (Palmen and Newton 1969),

$$\kappa_s = \kappa_t \frac{v}{(v - c)},$$

where v is the particle speed and c is the phase speed of the propagating meander. The speed of the floats was estimated from the change in position over a 16-hour period, using a simple centered-difference technique. Assuming the uncertainties in successive position fixes to be uncorrelated, the uncertainty in speed is given by $\sigma_v = \sqrt{2}\sigma_y/16$ hours. For $\sigma_y = \pm 5$ km, $\sigma_v = \pm 12$ cm s^{-1}. Since the uncertainty in successive fixes are probably correlated to some degree, reflecting common timing uncertainties, the above value represents an upper bound on the uncertainty of v.

Trajectory curvature was estimated as described by BR, and for uncorrelated position errors, has a mea-

surement uncertainty of about ±20% (again, probably an overestimate). An average value of $c = 8 \pm 12$ cm s^{-1} (Gilman 1988) for meanders between 73° and 60°W was used. (Estimates of c for each float could in principle be made from satellite IR imagery but excessive cloudiness makes this impractical for large numbers of floats.) For typical values of $v = 100$ cm s^{-1} and $\kappa_t = 0.01$ km^{-1}, standard propagation of errors (Bevington 1969) leads to an uncertainty in the estimate of κ_s of ± 0.0032 km^{-1}. The uncertainty in the product, $\kappa_s v$, is given by $(\sigma_{\kappa_s v}/\kappa_s v)^2 = (\sigma_{\kappa_s}/\kappa_s)^2 + (\sigma_v/v)^2$. Again for typical values of κ_s and v, the uncertainty in $\kappa_s v$ is estimated to be about $\pm 0.35 \times 10^{-5}$ s^{-1}.

Because the RAFOS floats are not perfectly isopycnal, they can become vertically separated from the fluid parcel originally tagged by as much as 40 m (BR). Given a vertical shear of 1×10^{-3} s^{-1} in the main thermocline (Table 1), this corresponds to a difference in speed of about 4 cm s^{-1} between the float and fluid parcel. For a typical meander with $\kappa_s = 0.01$ km^{-1}, the difference in curvature vorticity between the float and fluid parcel will be only 0.04×10^{-5} s^{-1}, which is much less than the measurement uncertainty estimated above. Thus the inability of a RAFOS float to exactly follow a fluid parcel is not significant in the estimate of curvature vorticity of the fluid parcel.

3) Lateral shear vorticity term

The RAFOS floats were launched in the Gulf Stream sequentially and not in clusters; therefore, it was not possible to observe changes in lateral shear directly. However, considerable information about the lateral (and vertical) structure of downstream speed in the Gulf Stream is available from the study by HR at 73°W. Using the velocity profiler PEGASUS, they completed 16 sections across the stream over a three-year period. Each section usually consisted of nine profiles of temperature and velocity from the sea surface to near the bottom spaced at 24 km intervals across the current. HR transformed each section into a natural coordinate system before constructing the mean sections shown in Fig. 1.

Lateral shear was estimated along the RAFOS trajectories by first determining the cross-stream position of the float using the float temperature and pressure in a model of the cross-stream thermal structure. The model, described in BR, is an exponential function which was fit subjectively to match the mean thermal structure shown in Fig. 1. Lateral shear at the cross-stream position of the float was then estimated by differentiating a sixth order polynomial which was fit to the PEGASUS mean speeds along the density surface of the float. In Fig. 2, an example of the mean speeds, the polynomial fit, and the cross-stream structure of lateral shear is illustrated for the 10°C surface. This function was used to estimate $\partial v/\partial n$ only between −50 and 60 km where it is well behaved.

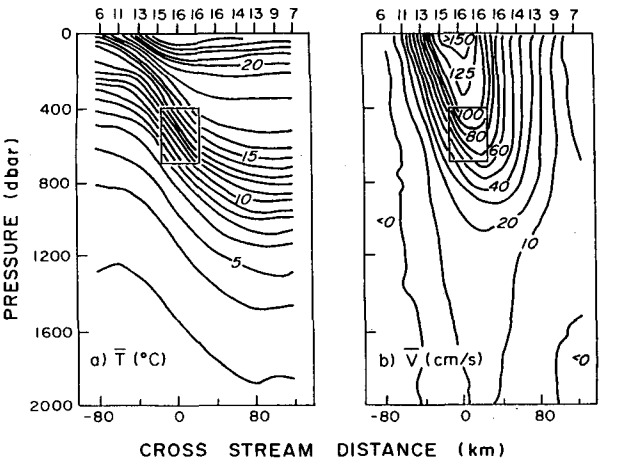

FIG. 1. Mean (a) temperature and (b) velocity sections in natural coordinates from the PEGASUS study at 73°W. Boxed areas indicate the portion of the Gulf Stream seeded with floats. Number of profiles used to construct the mean at each cross-stream location is indicated on top axis.

The method for estimating lateral shear assumes that the velocity structure of the Gulf Stream is independent of downstream distance. The basis for this assumption lies in the fact that many investigators have shown the structure to be quite similar at numerous locations along the current's path (Fuglister 1963; Richardson et al. 1969; HR; Leaman et al. 1989; Hendry 1988; BR). The HR study in particular pointed out how remarkably constant the velocity structure is when the sections are put in natural coordinates and the blurring effect of meandering is removed. HR reported typical standard deviations in velocity in the stream coordinate system to be about ±15 cm s^{-1} in the main thermocline (compared to ±30 cm s^{-1} in geographical coordinates). This variability in speed could still result in substantial variability in shear if velocity fluctuations at neighboring stations are uncorrelated. Fig. 3 shows, however, that the velocity fluctuations at neighboring stations are in fact positively correlated to a high degree, especially on the anticyclonic side of the stream. On the anticyclonic side ($x_1 > 0$, $x_2 > 0$), velocity variations are highly correlated ($\rho > 0.5$) over cross-stream length scales of about 35 km. On the cyclonic side ($x_1 < 0$, $x_2 < 0$), this scale is smaller, about 15 km.

An estimate of the variability in lateral shear for the main thermocline of the Gulf Stream was obtained by plotting lateral shear in the layer 10°–14°C as a function of cross-stream distance for each of the PEGASUS sections in stream coordinates (Fig. 4). This figure was constructed by first computing depth-averaged downstream speed between 10° and 14°C at each station, then using first-differences between stations to estimate lateral shear, and finally averaging the estimates in 20 km bins.

On the anticyclonic side of the stream, the estimates of $\partial v/\partial n$ cluster together, with standard deviations all

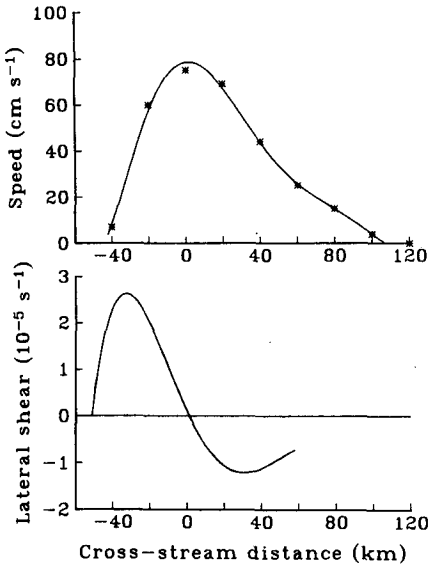

FIG. 2. (a) Mean speed on 10°C surface as function of cross-stream distance from PEGASUS mean section (symbols) with sixth-order polynomial fit (solid line); (b) cross-stream structure of lateral shear on 10°C surface, obtained by differentiating the function in (a).

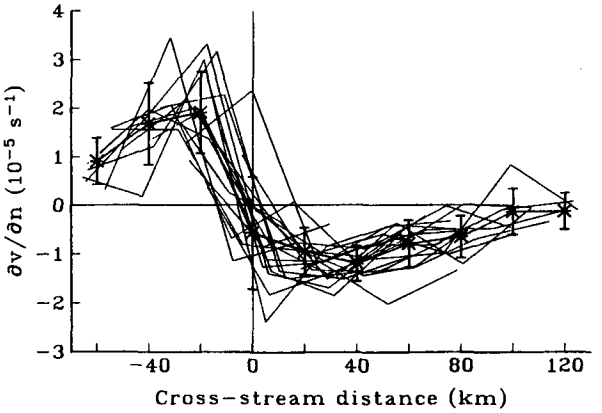

FIG. 4. Lateral shear in 10°–14°C layer as function of cross-stream distance for 20 PEGASUS sections. Symbols indicate the mean in 20 km bins and bars are standard deviations.

less than $\pm 0.5 \times 10^{-5}$ s^{-1}. On the cyclonic side, the variability appears to be much larger, with standard deviations reaching $\pm 1.0 \times 10^{-5}$ s^{-1}. However, some of this variability is probably due to 1) undersampling in a region of strong gradients of velocity and lateral shear, and 2) the somewhat crude first-difference technique used for estimating lateral shear in this figure. Thus the uncertainty in the estimate of lateral shear following the RAFOS floats is judged to be $\pm 0.5 \times 10^{-5}$ s^{-1}. The results will not be altered significantly if the uncertainty in lateral shear on the cyclonic side of the stream has been underestimated (see section 3 below).

An additional source of uncertainty arises from the fact that not much is known about how the velocity structure of the Gulf Stream changes in very sharply curved meanders. Float observations seem to indicate that the structure is very similar all along the stream regardless of path curvature (see Shaw and Rossby 1984; BR), however, there are very few hydrographic sections (especially orthogonal traverses) through such features to confirm these findings. This source of uncertainty must therefore remain until more experimental information is available.

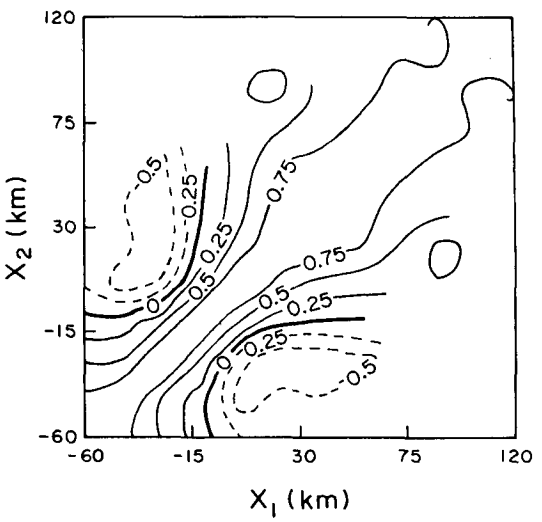

FIG. 3. Contour diagram of correlation coefficients ($\rho_{v(x_1)v(x_2)}$) between velocity fluctuations at given cross-stream location (x_2 axis) and fluctuations at other cross-stream positions (x_1 axis). Based on speed observations in 10°–14°C layer from 20 PEGASUS sections.

4) LAYER THICKNESS TERM

The layer thickness changes of the tagged parcel were determined assuming potential vorticity is conserved. The potential vorticity of the floats was estimated to be 1×10^{-6} m^{-1} s^{-1} based on the cross-section of potential vorticity at Cape Hatteras constructed by Leaman et al. (1989). They show that potential vorticity is quite uniform in the 10°–14°C layer in the center of the stream. This value for potential vorticity is associated with an initial vertical scale for the fluid parcel of 70–80 m, which is approximately the vertical distance between density surfaces differing by 0.2 σ units in the main thermocline of the Gulf Stream. Estimates of H were made at 8 hour intervals by dividing absolute vorticity by the constant. The uncertainty in the estimate of H, given by $\sigma_H = \sigma_{\xi_a}/\text{constant}$, is then $\sigma_H = \pm 0.6 \times 10^{-5}\ \text{s}^{-1}/1.0 \times 10^{-6}\ \text{m}^{-1}\ \text{s}^{-1} = \pm 6$ m. Uncertainties for each component of potential vorticity are summarized in Table 3.

TABLE 3. Uncertainties in potential vorticity terms.

Component	Estimated uncertainty
f	$\pm 0.01 \times 10^{-5}$ s^{-1}
$\kappa_s v$	$\pm 0.35 \times 10^{-5}$ s^{-1}
$\partial v/\partial n$	$\pm 0.5 \times 10^{-5}$ s^{-1}
ζ_a	$\pm 0.6 \times 10^{-5}$ s^{-1}
H	± 6 m

c. *Estimation of horizontal divergence following RAFOS floats*

Horizontal divergence was estimated from the average time rate of change of absolute vorticity between meander extrema according to:

$$\frac{\partial w}{\partial z} = \frac{1}{H}\frac{dH}{dt} = \frac{1}{\zeta_a}\frac{d\zeta_a}{dt} \approx \frac{1}{\frac{1}{2}(\zeta_{a_e} + \zeta_{a_b})}\frac{(\zeta_{a_e} - \zeta_{a_b})}{\Delta t} \quad (4)$$

where ζ_{a_b} and ζ_{a_e} are the absolute vorticity at the beginning and end of the trajectory segment and Δt is the time required for the float to transit the segment. Uncertainties in the divergence estimates are a function of ζ_a and Δt and will be discussed along with the results in the next section.

3. Results

a. *Potential vorticity balances*

In the first half of this section, the potential vorticity balances for two individual drifters, RAFOS 020 and RAFOS 022, will be examined. Figure 5 shows the trajectory, temperature, and pressure records for RAFOS 022. It was launched in October 1984 off Cape Hatteras and drifted downstream for 30 days with an average speed of 67 cm s^{-1}. From the temperature record, it can be seen that this float was neutrally buoyant on the 10°C surface ($\sigma_t = 27.2$) with deviations from that surface less than ±1°C. The striking pattern of vertical motion mentioned in the Introduction is particularly evident if one compares the pressure record with the trajectory. The drifter consistently downwelled as it traveled from crest to trough (e.g., yeardays 287–292) and upwelled between trough and crest (e.g., 292–297).

As pointed out by BR, a vertical component of motion implies an accompanying lateral or cross-stream component since the floats are confined to an isopycnal (or isothermal) surface. The cross-stream position of the float as a function of time (Fig. 6) has been estimated from the model of the mean thermal structure

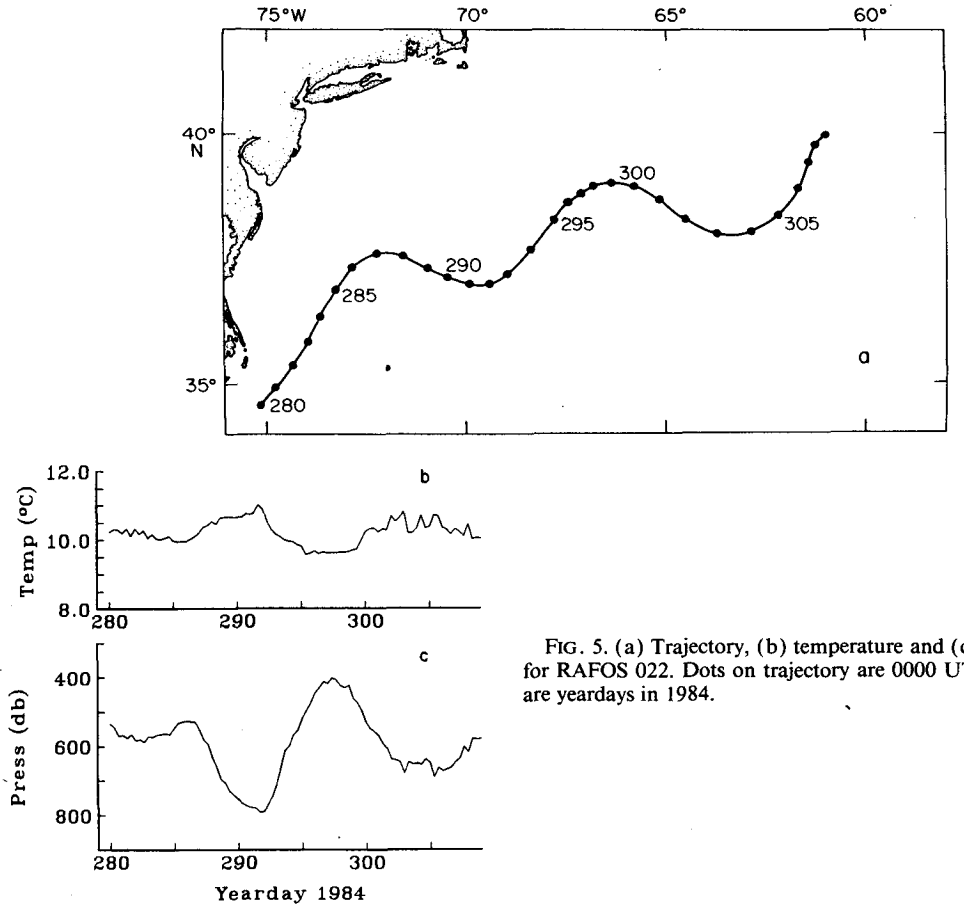

FIG. 5. (a) Trajectory, (b) temperature and (c) pressure records for RAFOS 022. Dots on trajectory are 0000 UTC fixes and dates are yeardays in 1984.

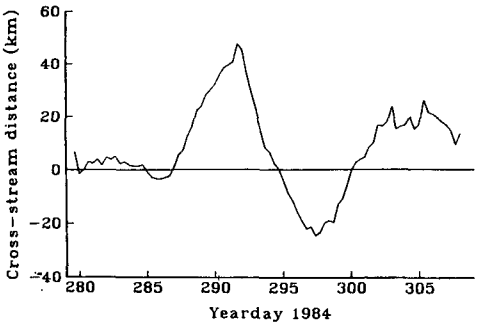

FIG. 6. Cross-stream position of RAFOS 022 as function of time along trajectory. Positive (negative) values indicate offshore (onshore) displacements.

(see BR) of the stream. The origin is taken to be where the 12°C isotherm intersects 500 m (high speed core). This figure indicates that the float was launched very near the center of the stream ($\partial v/\partial n \approx 0$) where it remained until yearday 285. After that point, the float began oscillating back and forth across the stream as it flowed along the wavelike path of the current. The largest cross-stream excursion took place between yeardays 292 and 297, when the float moved 70 km laterally, from 45 to −25 km, over 5 days.

The components of potential vorticity for RAFOS 022 are shown in Fig. 7 as a function of time along the trajectory. The scale for each of the terms in the absolute vorticity is the same so that relative changes can easily be discerned. Planetary vorticity changed little compared to curvature and lateral shear vorticity. The curvature vorticity, which had peak values about 10% of f, alternated sign according to changes in sign of the trajectory curvature (positive in cyclonic meander troughs, negative in anticyclonic meander crests).

Lateral shear vorticity showed the largest changes of these first three components; this is due to the large lateral displacements of the float *relative* to the jet. Comparing this plot to Fig. 6, we see that when the float moved offshore away from the center of the stream (e.g., 287–292), the speed of the float decreased (not shown) and lateral shear became negative. Similarly, the float speed decreased and lateral shear became positive as the float moved onshore (e.g., 295–297). The asymmetry of the velocity structure along the 10°C surface (see Fig. 2) implies that shears are considerably greater on the cyclonic flank of the stream than on the anticyclonic flank.

The final panel in Fig. 7 shows the changes in layer thickness of the tagged fluid parcel, estimated from the changes in absolute vorticity. Up until yearday 293, changes in H were generally less than ±10% due to the fact that $\kappa_s v$ and $\partial v/\partial n$ were at least partially compensating. The most dramatic increase in H occurred between yeardays 292 and 297. This corresponds to the time when the float was displaced laterally by 70 km as it approached a meander crest. This lateral displacement brought the float well into the cyclonic shear zone of the stream where it reached the maximum shear for this temperature surface (see Fig. 2). As a result of this large increase in absolute vorticity, the layer thickness must also increase to maintain constant potential vorticity. As the float moved away from the cyclonic shear zone in the next half wavelength, the layer thickness decreased back to its original value.

It is important to examine this 30% change in layer thickness more carefully to ensure that such a large change is in fact reasonable. The two quantities which are estimated directly from the RAFOS data, f and $\kappa_s v$, together show a change of -0.84×10^{-5} s^{-1} between yeardays 292 and 297. In order to compensate exactly for this change which would imply no change in layer thickness at all, only a $+0.84 \times 10^{-5}$ s^{-1} increase in lateral shear vorticity is necessary. Figure 8 shows the mean PEGASUS velocity section with the 10°C isotherm mean position and the cross-stream excursion of RAFOS 022 between yeardays 292 and 297 superimposed. Using this mean section, the change in lateral shear experienced by the float was estimated to be $+3.1 \times 10^{-5}$ s^{-1}, or four times larger than the change which would have left H constant.

It seems unlikely that the velocity structure could alter in such a way as to reduce the change in shear experienced by this float by a factor of four. Examples of the basic structural changes which would be required at both the trough and crest are a fourfold increase in

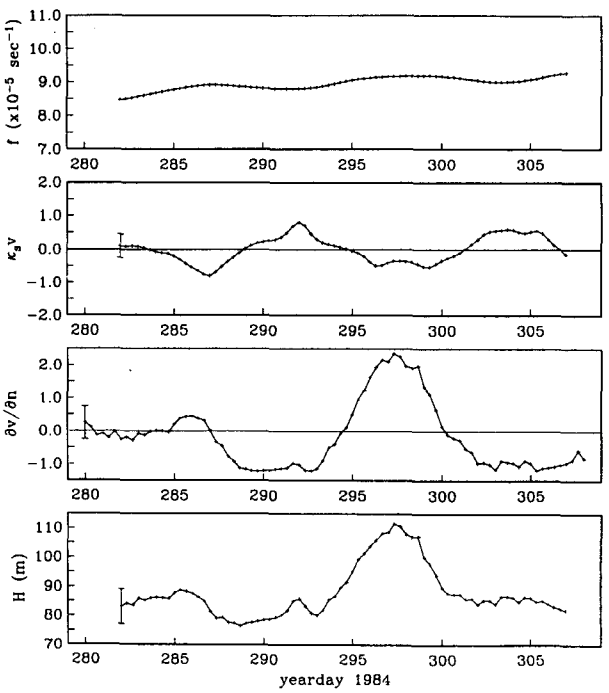

FIG. 7. Potential vorticity terms for RAFOS 022 as function of time along the trajectory. Units for top three panels are 10^{-5} s^{-1}. Bars indicate uncertainty limits.

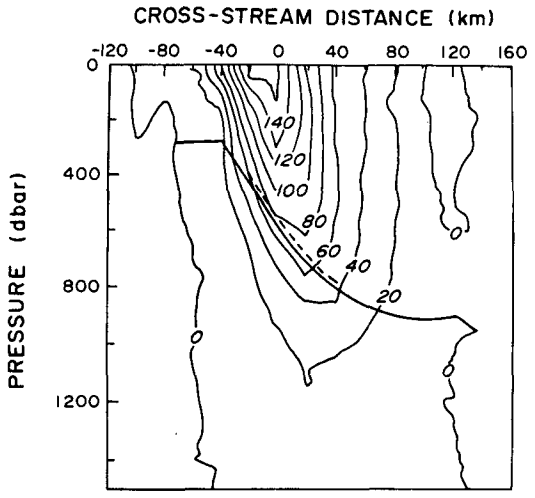

FIG. 8. Mean velocity section in natural coordinates from PEGASUS study with mean position of 10°C isotherm and cross-stream excursion of RAFOS 022 superimposed.

the width of the stream, or a 75% drop in the peak speed in the center of the current. Such drastic changes in the subsurface structure of the Gulf Stream have not been observed in previous studies (Richardson et al. 1969; Shaw and Rossby 1984; HR; Hendry 1988; BR), so it seems quite certain that the thickness of the fluid parcel tagged by RAFOS 022 did in fact increase as the float approached a meander crest.

While the above results are typical for floats which crossed into the cyclonic shear zone, quite different results are obtained from floats which remained only on the anticylonic side of the stream. RAFOS 020 is a clear example of such a float. In Fig. 9, the trajectory, temperature, and pressure records are shown for this float, which was launched off Cape Hatteras in August 1984. RAFOS 020 also had a fairly simple trajectory until yearday 247 when the float entered a warm core ring which was interacting with the stream (visible in satellite IR imagery). In the pressure record, the ubiquitous pattern of upwelling and downwelling is again evident. (The high visual correlation between the temperature and pressure records is due to the fact that the float is slightly less compressible than seawater.) Note that the systematic pattern of vertical motion was absent during the early straight section of the trajectory and after the float entered the ring.

The record of the float's cross-stream position is shown in Fig. 10. This float was launched about 10 km offshore from the center of the stream, and remained on the anticyclonic side of the stream for its entire

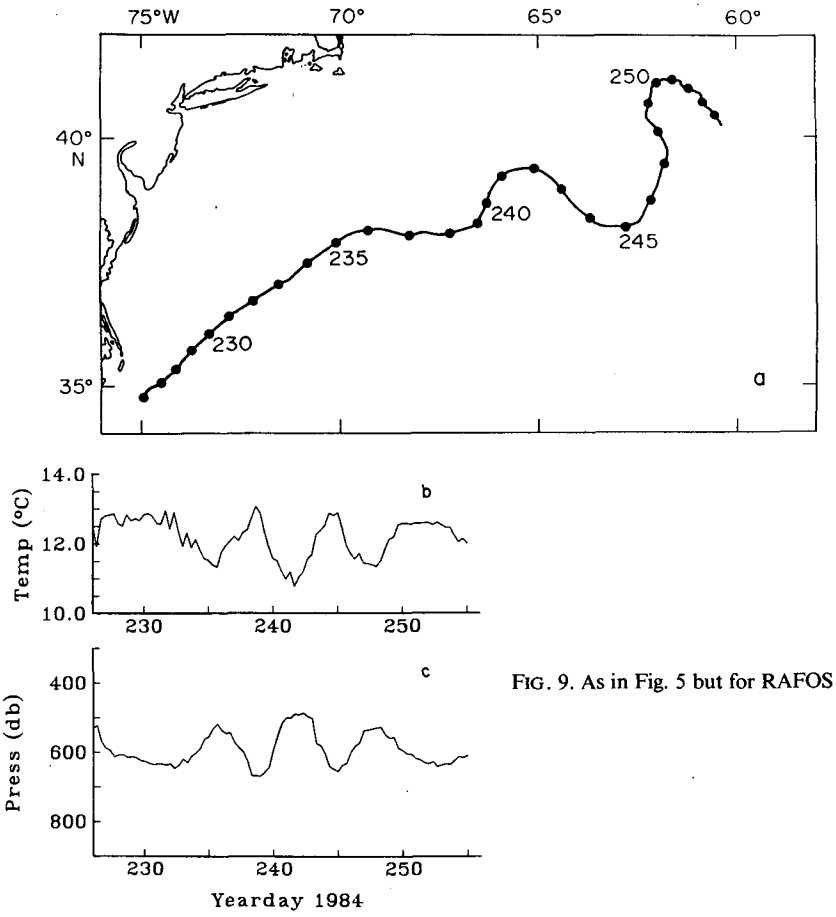

FIG. 9. As in Fig. 5 but for RAFOS 020.

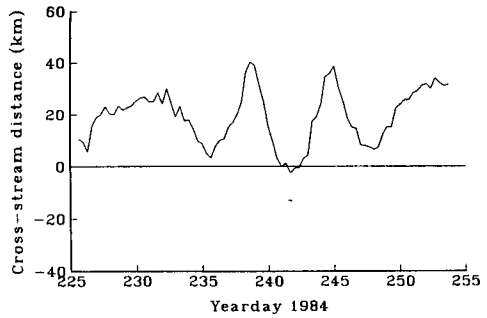

FIG. 10. As in Fig. 6 but for RAFOS 020.

mission. The lateral displacements of this float are also highly correlated with changes in curvature of the trajectory as was the case for RAFOS 022.

The potential vorticity components for RAFOS 020 are presented in Fig. 11. As before, f did not change as much as $\kappa_s v$ and $\partial v/\partial n$ on the meander time scale, although the planetary vorticity did increase about 10% up to day 247. Unlike the previous example, however, this float did not cross into the cyclonic shear zone, and thus there were no large positive shears experienced by this float. In fact, curvature and shear vorticity compensate for each other almost completely, and layer thickness changes are quite small. Although the signal is weak, there is some indication that the layer thickness changes follow the changes in curvature vorticity. Except for the first half-wavelength (yeardays 233–236), the float experienced increasing layer thickness between a crest and a trough (yeardays 236–239) and decreasing layer thickness between trough and crest (yeardays 239–242). Other floats on the anticyclonic side show larger changes in H which follow the changes in curvature vorticity (see following subsection).

These two representative examples suggest that fluid parcels in the midthermocline approaching meander crests on the anticyclonic side of the current experience a slight decrease in layer thickness, while fluid parcels which cross into the cyclonic shear zone as they approach meander crests experience increasing layer thickness. The opposite pattern is observed on approach to meander troughs.

b. *Divergence estimates in the Gulf Stream*

Horizontal divergence was estimated by breaking the trajectories into segments between meander crests and troughs. If a float was observed to escape from the stream along a particular segment, no divergence estimate was made for that segment. Sixty-one estimates of divergence were made in all from 24 trajectories between 75° and 55°W.

The divergence estimates were first divided into two groups depending on whether the segment was from a trough to a crest or vice versa. The estimates were further divided into right and left side of the stream. Segments where the float remained exclusively on the anticyclonic side of the current were put in the right side group, while segments where the float crossed into the cyclonic shear zone by any amount were put in the left side group.

Figures 12a–d illustrate the divergence estimates for each group as a function of temperature with uncertainty limits indicated for each estimate. All four groups show a tendency for larger absolute values of $\partial w/\partial z$ on shallower density surfaces. The more striking feature, however, is the distinct difference in sign of $\partial w/\partial z$ on either side of the Gulf Stream. Looking first at Figs. 12a and 12b for downstream of a trough, floats on the right side of the stream experienced primarily horizontal *divergence* ($\partial w/\partial z < 0$), while most floats which crossed into the cyclonic shear zone underwent horizontal *convergence* ($\partial w/\partial z > 0$). A similar difference in sign was observed downstream of a crest, Figs. 12c and d, but in the opposite sense. On the anticyclonic (right) side of the stream, a majority of the estimates indicate horizontal *convergence,* while on the cyclonic (left) side, primarily horizontal *divergence* is indicated.

In each of the four groups, a weighted mean of $\partial w/\partial z$ was estimated for the 10°–14°C layer (the layer with the most estimates) according to

$$\mu' = \frac{\sum_1^n \frac{x_i}{\sigma_i^2}}{\sum_1^n \frac{1}{\sigma_i^2}}$$

where x_i and σ_i represent each divergence estimate and its associated uncertainty (Bevington 1969). Similarly,

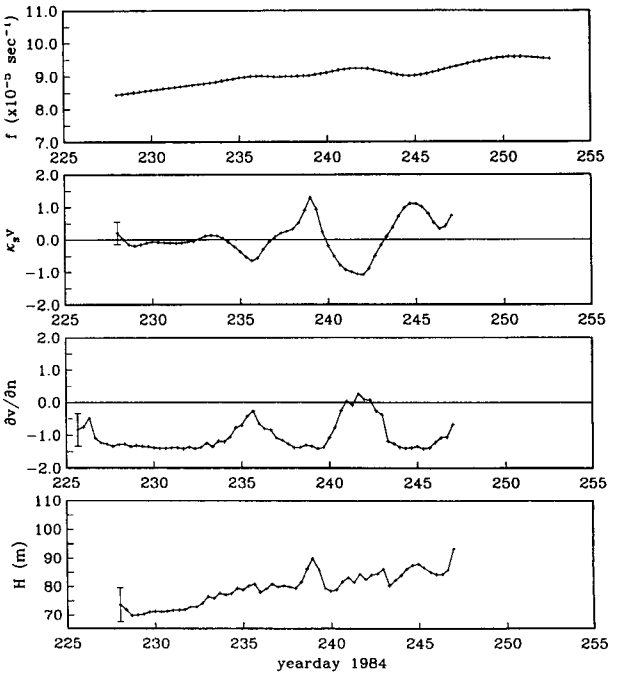

FIG. 11. As in Fig. 7 but for RAFOS 020.

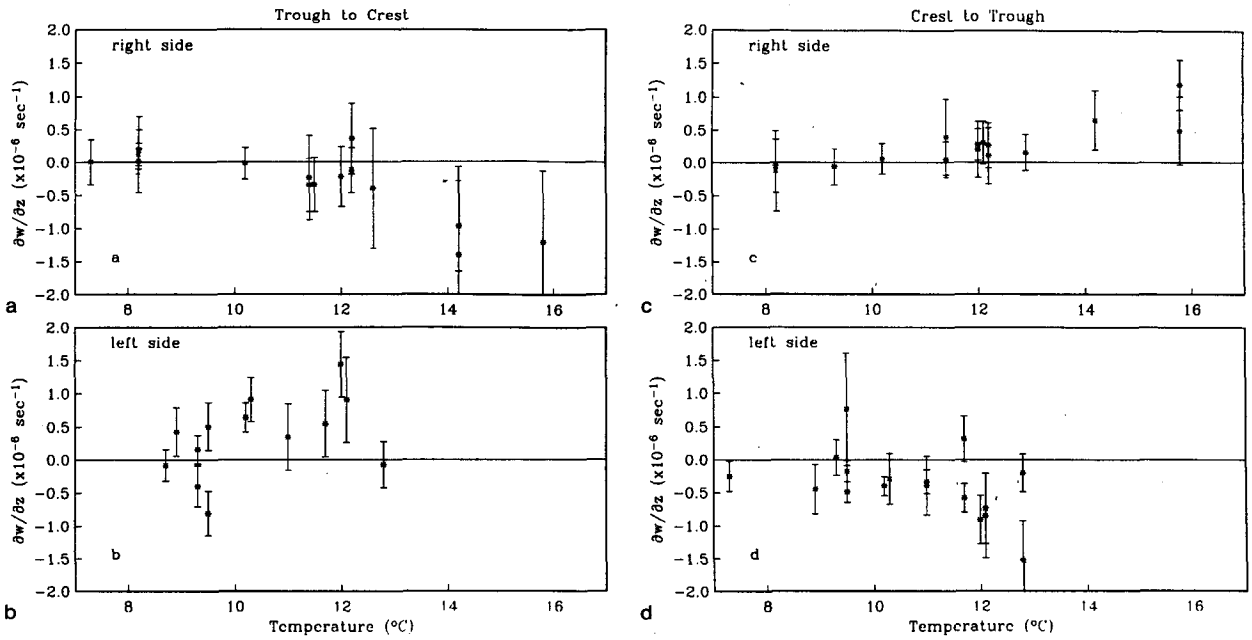

FIG. 12. Estimates of horizontal divergence based on RAFOS float observations as a function of temperature in four regions of Gulf Stream meanders: (a) floats drifting from trough to crest, right-hand side of current; (b) same as (a) but for left side; (c) floats drifting from crest to trough, right-hand side of current; (d) same as (c) but for left side.

the estimated error in the mean (standard error) was calculated according to

$$\sigma_\mu{}^2 = 1 \Big/ \sum_1^n \frac{1}{\sigma_i^2}.$$

These results and the standard deviation of the observations are listed in Table 4. Based on a Student's t-distribution with $n - 1$ degrees of freedom, the estimates of the mean on the left side of the stream are significantly different from 0 at the 99% confidence level. On the right side the confidence levels for nonzero divergence are less; 80% downstream of a crest (Fig. 12c) and only 50% downstream of a trough (Fig. 12a). The smaller values (absolute) of $\partial w/\partial z$ on the right side reflect the near balance between curvature vorticity and lateral shear vorticity changes at this level, although the former appears to dominate slightly, especially on shallower temperature surfaces. On the cyclonic side, the strong dominance of the lateral shear vorticity changes is evident in the larger mean values on that side. These results are summarized schematically in Fig. 13.

TABLE 4. Estimates of mean divergence in Gulf Stream meanders (10°–14°C layer) (Units are 10^{-6} s^{-1}.)

	Trough to crest		Crest to trough	
Statistic	Left	Right	Left	Right
μ'	.618	−.126	−.409	.176
sd	.444	.229	.450	.112
σ_μ	.138	.141	.082	.104
n	7	8	11	9

4. Discussion

The time series of potential vorticity terms following RAFOS floats revealed that fluid parcels in the main thermocline of the Gulf Stream experience changes in curvature and lateral shear vorticity which are large compared to the changes in f, the planetary vorticity. In fact, the changes in f are so small as to be nearly insignificant in the balance of terms following individual fluid parcels.

It is interesting to compare these results to the steady-state free inertial jet model developed by Robinson

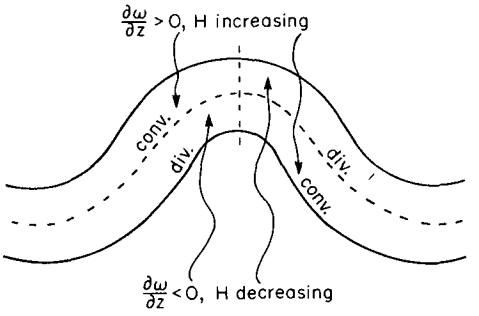

FIG. 13. Schematic view of Gulf Stream meander showing regions of convergence and divergence on representative density surface in the main thermocline.

and Niiler (1967, hereafter RN). They derived an expression for the downstream change in jet path curvature by integrating the vorticity equation [steady-state version of Eq. (4)] in the cross-stream plane (x, z) and applying the following scaling restrictions: (i) jet must be vertically coherent, (ii) the radius of curvature of the path must always be greater than the width of the jet, and (iii) horizontal divergence must be small over distances comparable to the width of the jet. The second condition is equivalent to the restriction that changes in bottom depth be small compared to the mean bottom depth.

The expression for path curvature is [RN Eq. (3.8)]

$$\frac{\partial}{\partial y}\left[\langle v^2\rangle\kappa\right] + \langle v\rangle\beta\sin\theta + f_0\bar{v}S(y) = 0, \quad (5)$$

(A) (B) (C)

where

θ angle current makes with east,
S bottom slope along jet,
$\langle\ \rangle$ integration in x, z plane,
$(\ )$ integration in x at sea bottom.

This equation states that downstream changes in the quantity $\langle v^2\rangle\kappa$ are governed by a combination of beta and topographic effects [terms B and C, respectively]. For a jet of constant transport, Eq. (5) can be integrated once in y to give the path curvature as a function of transport, initial curvature, bottom velocity, and bottom slope.

In the Gulf Stream region east of 70°W, the bottom slope experienced by the current is quite small (excluding the seamounts), and scaling analysis shows that, in general, term B dominates over term C when the jet is meandering ($\theta \neq 0$). Let $\langle v\rangle \approx 100 \times 10^6$ $m^3\,s^{-1}$, $\beta \approx 1.8 \times 10^{-11}\,m^{-1}\,s^{-1}$, $\theta \approx 45°$ (NE flow), $\bar{v} \approx$ (5–10 cm s^{-1}) × (80 km), and $S \approx 10^{-3}$–10^{-4}. The ratio of topographic to beta terms (C/B) is then in the range 0.03–0.63, implying that in this region the Gulf Stream path is governed primarily by the beta effect and the influence of topography is of secondary importance.

In light of these observations, it is somewhat surprising that variations in the planetary vorticity term are of relatively little importance in the vorticity balance following the RAFOS floats, while lateral shear vorticity changes, which do not even appear in Eq. (5), are so large. There is however, an important difference in these two views of the governing dynamics; the curvature of the jet *path* will be determined by the integrated dynamical response of all fluid parcels in the jet while the balance of terms following RAFOS floats represents the dynamical adjustment of individual fluid parcels. In particular, the large changes in shear vorticity which balance the divergence following some fluid parcels (e.g., RAFOS 022) will not be important when integrated over all fluid parcels since $v \to 0$ at the edges of the jet. Likewise the changes in planetary vorticity are insignificant for individual parcels but are of critical importance when integrated over all parcels.

Although it is the integral vorticity properties of the Gulf Stream which appear to be important for determining its path, the RAFOS float observations provide information on the horizontal and vertical structure of the terms of potential vorticity. Looking first at the horizontal structure, the pattern illustrated in Fig. 13 suggests that on the anticyclonic side of the stream curvature vorticity changes dominate slightly over lateral shear vorticity changes and the sign of $\partial w/\partial z$ follows the sign of $d(\kappa_s v)/dt$. However, when fluid parcels cross into the highly sheared region on the cyclonic side of the jet, lateral shear vorticity changes dominate and the sign of $\partial w/\partial z$ follows that of

$$\frac{d}{dt}\left(\frac{\partial v}{\partial n}\right).$$

The estimates of $\partial w/\partial z$ in Figs. 12a–d also give some indication of the vertical structure of horizontal divergence. On the anticyclonic side, the absolute value of $\partial w/\partial z$ decreases with decreasing temperature to near zero below 10°C. This "level of nondivergence" (LND) corresponds to the level where changes in curvature vorticity exactly balance changes in lateral shear vorticity (for f constant). The absolute value of w will have a maximum at this level. Hall (1986) inferred a LND in the Gulf Stream at 875 m based on estimates of vertical velocity at a moored current meter site. This is about the depth of the 8°C isotherm in the middle of the stream (see Fig. 1).

Above the LND, $|\partial w/\partial z|$ increases upward, most likely reaching a maximum in the surface layers where w must go the 0 to satisfy the sea surface boundary condition. On the cyclonic side, it is anticipated that the sign of $\partial w/\partial z$ switches as one goes up in the water column such that the *average* value of $\partial w/\partial z$ above a float on that side will have the same sign as on the anticyclonic side (see Fig. 14). This pattern is consistent with the observed *upward* motion of floats on both sides of the current (downstream of a trough), but is should be considered as one of several possibilities at this time. More observations are needed in the layers above the main thermocline to confirm the suggested pattern.

In this study, the RAFOS float observations have been used primarily to determine the sign of horizontal divergence in Gulf Stream meanders. Although the magnitudes are less certain, due mostly to the uncertainty in estimating $\partial v/\partial n$ following the floats, the estimates shown in Fig. 12 at least give upper and lower limits for $\partial w/\partial z$ in the main thermocline. The largest values (absolute) estimated are on the order of $1.5 \times 10^{-6}\,s^{-1}$ (1.7% of f). Mean values for the 10°–14°C layer are more on the order of $0.5 \times 10^{-6}\,s^{-1}$ (left side, 0.6% of f) and $0.15 \times 10^{-6}\,s^{-1}$ (right side, 0.2% of f) between meander extrema.

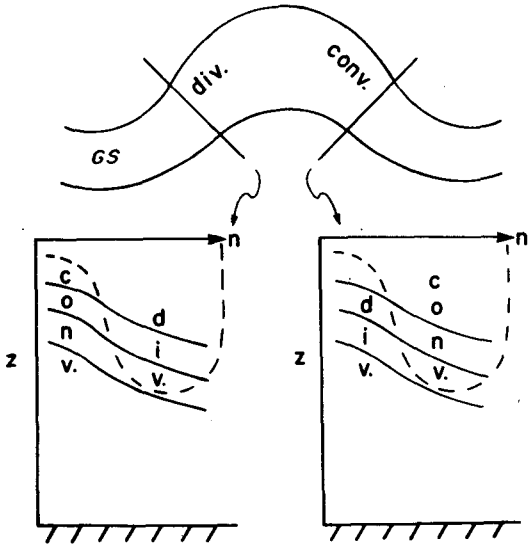

FIG. 14. Schematic view of two sections across the Gulf Stream showing vertical and cross-stream structure of divergence based on the RAFOS observations. See text for explanation.

These estimates of horizontal divergence and layer thickness changes can be used to examine the validity of the quasi-geostrophic approximation in Gulf Stream flow. This approximation requires that, over length scales comparable to the radius of deformation, fractional layer thickness changes must be much less than 1 (e.g., Stern 1975). This is clearly not the case according to the RAFOS observations; some fluid parcels tagged with floats experienced 30% layer thickness changes between meander extrema (e.g., see Fig. 7). Although these changes take place over *downstream* length scales of 100–200 km, which are long compared to the internal deformation radius ($\approx$45 km), the fluid parcels also move across the jet distances on the order of 20–70 km. It is this cross-stream length scale which is relevant to quasi-geostrophic theory. Based on these results, therefore, the quasi-geostrophic approximation appears to be inappropriate for use in modeling the Gulf Stream; Hall (1986) has also made this point based on several estimates of the Rossby number.

5. Summary

Thirty-seven RAFOS floats launched in the center of the Gulf Stream off Cape Hatteras have been analyzed to examine the dynamics of Gulf Stream meanders from a Lagrangian viewpoint. The floats show a systematic pattern of vertical and cross-stream motion in the main thermocline which is directly related to the meanders of the Gulf Stream path. Fluid parcels at this level are observed to upwell (downwell) and move onshore (offshore) downstream of meander troughs (crests).

The individual terms that make up the potential vorticity were estimated following two particular floats. These records show that curvature and lateral shear vorticity, as well as vortex stretching, vary significantly following fluid parcels in the main thermocline of the Gulf Stream. In one example, changes in layer thickness were primarily balanced by changes in lateral shear as the float made large excursions into the cyclonic shear zone of the current. In the second example, where the float remained on the anticyclonic flank of the stream, the layer thickness changes, although weak, reflected changes in curvature vorticity.

Sixty-one estimates of horizontal divergence following the RAFOS floats were made from the time rate of change of absolute vorticity along the trajectories. Values as high as $(\pm)1.5 \times 10^{-6}$ s^{-1} were observed on the upper density surfaces of the main thermocline between meander extrema, with values decreasing with increasing depth. On the anticyclonic side of the stream, horizontal divergence (convergence) was observed downstream of meander troughs (crests), while on the cyclonic side, the pattern was reversed.

These results suggest that there is a three-way dynamical balance following individual fluid parcels in Gulf Stream meanders between curvature and shear vorticity and vortex stretching. For the Gulf Stream as a whole, the primary balance is two-way between curvature and planetary vorticity changes.

The observations of vertical velocity and divergence have been combined with the surface boundary condition ($w = 0$ at $z = 0$) to construct a possible configuration of the cross-stream and vertical structure of horizontal divergence. The result resembles a two-layer system with upper-level divergence and lower-level convergence downstream of troughs separated by a layer of maximum vertical motion in the lower main thermocline (opposite downstream of crests). Fractional changes in layer thickness are large enough to challenge the appropriateness of using the quasi-geostrophic approximation to model the Gulf Stream.

Acknowledgments. The author gratefully acknowledges J. Lillibridge and R. O'Gara for assistance in software development, and H. Soiland for making available his analysis of the PEGASUS velocity data. Helpful discussions with T. Rossby, R. Watts, and J. Merrill contributed to the development of the ideas presented in this paper. Careful reading by one reviewer was especially helpful in getting the manuscript into final form. This work was supported by ONR Contract N00014-81-C-0062 to Dr. Tom Rossby at the University of Rhode Island.

APPENDIX A

Estimate of Eddy Diffusive Terms in Potential Vorticity Equation

The diffusive terms which have been neglected on the rhs of Eq. (1) are

$$K_H \nabla^2_H(\mathrm{PV}) + K_z \frac{\partial^2}{\partial z^2}(\mathrm{PV})$$

where

K_H, K_z = horizontal, vertical eddy diffusivities,

$$\nabla^2{}_H = \frac{\partial^2}{\partial x^2} + \frac{\partial^2}{\partial y^2},$$

$$\mathrm{PV} = \vec{\zeta}_a \cdot \frac{\nabla \rho}{\rho}.$$

After transforming these terms to a natural coordinate system and scaling analysis (see section 2 for more details), it can be shown that the largest term by far in the Gulf Stream involves the cross-stream gradient of potential vorticity,

$$K_H \frac{\partial^2}{\partial n^2}(\mathrm{PV}),$$

where n is the cross-stream coordinate directed along density surfaces.

Leaman et al. (1989) have examined the cross-stream structure of potential vorticity along temperature surfaces at three locations along the Gulf Stream path. They show that in the main thermocline the anticyclonic side of the current is characterized by almost uniform potential vorticity along temperature surfaces $[\partial(\mathrm{PV})/\partial n = 0]$. On the cyclonic side, the gradient of potential vorticity on the 12°C surface for example, is approximately 1.0×10^{-11} m^{-2} s^{-1} (see Leaman et al. Fig. 10b). For a crude estimate of $\partial^2(\mathrm{PV})/\partial n^2$, we can take $[\partial(\mathrm{PV})/\partial n$ (cyclonic side) $- \partial(\mathrm{PV})/\partial n$ (anticyclonic side)$]/5$ km $= 2.0 \times 10^{-15}$ m^{-3} s^{-1}, where 5 km is judged to be the diffusive length scale for the fluid parcels tagged by the RAFOS floats. Using the value for K_H of 1.0×10^5 cm^2 s^{-1} reported by Schmitt and Georgi (1982) for diffusive processes on scales of 1–5 km, $K_H(\partial^2/\partial n^2)(\mathrm{PV}) \approx 2 \times 10^{-14}$ m^{-1} s^{-2}, or 1.7×10^{-9} m^{-1} s^{-1} d^{-1}. For PV $\approx 1.0 \times 10^{-6}$ m^{-1} s^{-1}, this represents a 0.17% increase in PV per day or a 5% increase over 30 days. As is shown in section 3 of this work, fluid parcels traveling between meander troughs and crests on time scales of 5–10 days experience very large variations in the terms which make up potential vorticity, on the order of 10–50% (except f, the planetary vorticity). So for the purposes of this study, where we are examining potential vorticity balances over time scales of less than one month, potential vorticity is conserved.

REFERENCES

Bevington, P. R., 1969: *Data Reduction and Error Analysis for the Physical Scientist.* McGraw-Hill, 336 pp.

Bjerknes, J., and J. Holmboe, 1944: On the theory of cyclones. *J. Meteor.*, **1**, 1–22.

Bower, A. S., and T. Rossby, 1989: Evidence of cross-frontal exchange processes in the Gulf Stream based on isopycnal RAFOS float data. *J. Phys. Oceanogr.*, **19**, 1177–1190.

Ertel, H., 1942: Ein neuer hydrodynamischer Wirbelsatz. *Meteor. Z.*, **59**, 277–282.

Fuglister, F. C., 1963: Gulf Stream '60. *Progress in Oceanography*, Vol. 1, Pergamon, 265–373.

Gilman, Craig S., 1988: A study of the Gulf Stream downstream of Cape Hatteras 1975–1986. Master's thesis, University of Rhode Island, Graduate School of Oceanography, 77 pp.

Halkin, D., and T. Rossby, 1985: The structure and transport of the Gulf Stream at 73°W. *J. Phys. Oceanogr.*, **15**, 1439–1452.

Hall, Melinda, 1986: Horizontal and vertical structure of the Gulf Stream velocity field at 68°W. *J. Phys. Oceanogr.*, **16**, 1814–1828.

Hendry, R., 1988: A simple model of the Gulf Stream thermal structure with application to analysis of moored measurements in the presence of mooring motion. *J. Atmos. Oceanic Technol.* **5**(2), 328–339.

Holton, J. R., 1979: *An Introduction to Dynamic Meteorology*, 2nd ed., Academic Press, 391 pp.

Leaman, K., E. Johns and T. Rossby, 1989: The average distribution of volume transport and potential vorticity with temperature at three sections across the Gulf Stream. *J. Phys. Oceanogr.*, **19**(1), 36–51.

Newton, C. W., 1978: Fronts and wave disturbances in Gulf Stream and atmospheric jet stream. *J. Geophys. Res.*, **83**(C9), 4697–4706.

Palmen, E., and C. W. Newton, 1969: *Atmospheric Circulation Systems.* Academic Press, 603 pp.

Richardson, W. S., W. J. Schmitz and P. P. Niiler, 1969: The velocity structure of the Florida Current from the Straits of Florida to Cape Fear. *Deep-Sea Res.*, **16**(Suppl.), 225–231.

Robinson, A. R., and P. P. Niiler, 1967: The theory of free inertial currents: I. Path and structure. *Tellus*, **19**, 269–291.

Rossby, H. T., E. R. Levine and D. N. Connors, 1985: The isopycnal Swallow float–A simple device for tracking water parcels in the ocean. *Progress in Oceanography*, Vol. 14, Pergamon, 511–525.

——, D. Dorson and J. Fontaine, 1986: The RAFOS system. *J. Atmos. Oceanic Technol.*, **3**, 672–679.

Schmitt, R. W., and D. T. Georgi, 1982: Finestructure and microstructure in the North Atlantic Current. *J. Mar. Res.*, **40**(Suppl.), 659–705.

Shaw, P.-T., and H. T. Rossby, 1984: Towards a Lagrangian description of the Gulf Stream. *J. Phys. Oceanogr.*, **14**, 528–540.

Stern, M., 1975. *Ocean Circulation Physics.* Academic Press, 246 pp.